The Meteoritical Society

Meteoritics & Planetary Science 58, Nr 9, 1318–1332 (2023)
doi: 10.1111/maps.14058

Petrology and mineralogy of volcanic glass in meteorite Northwest Africa 11801: Implications for their petrogenesis

Guozhu CHEN[1,2], Zhipeng XIA[1,2]*, Bingkui MIAO[1,2]*, Zilong WANG[3,4]*, Wei TIAN[3], Yikai ZHANG[1,2], Hao LIU[1,2], Chuangtong ZHANG[1,2], Lanfang XIE[1,2], Yanhua PENG[1,2], Hongyi CHEN[1,2], and Xi WANG[1,2]

[1]Institution of Meteorites and Planetary Materials Research, Key Laboratory of Planetary Geological Evolution, Education Department of Guangxi Zhuang Autonomous Region, Guilin University of Technology, Guilin, China
[2]Guangxi Key Laboratory of Hidden Metallic Ore Deposits Exploration, Guilin University of Technology, Guilin, China
[3]Key Laboratory of Orogenic Belts and Crustal Evolution, School of Earth and Space Sciences, Ministry of Education, Peking University, Beijing, China
[4]Key Laboratory of Paleomagnetism and Tectonic Reconstruction of MNR, Institute of Geomechanics, Chinese Academy of Geological Sciences, Beijing, China
***Correspondence**
Zhipeng Xia and Bingkui Miao, Key Laboratory of Planetary Geological Evolution, Education Department of Guangxi Zhuang Autonomous Region, Institution of Meteorites and Planetary Materials Research, Guilin University of Technology, Guilin 541004, China.
Email: xiazhipeng@glut.edu.cn and miaobk@glut.edu.cn.
Zilong Wang, Key Laboratory of Orogenic Belts and Crustal Evolution, School of Earth and Space Sciences, Ministry of Education, Peking University, Beijing 100871, China.
Email: zilong.wang@pku.edu.cn

(Received 21 October 2022; revision accepted 13 July 2023)

Abstract–The study of lunar magma evolution holds significant importance within the scientific community due to its relevance in understanding the Moon's thermal and geological history. However, the intricate task of unraveling the history of early volcanic activity on the Moon is hindered by the high flux of impactors, which have substantially changed the morphology of pristine volcanic constructs. In this study, we focus on a unique volcanic glass found in the lunar meteorite Northwest Africa 11801. This kind of volcanic glass is bead-like in shape and compositionally similar to the Apollo-14 and Apollo-17 very low-Ti glass. Our research approach involves conducting a comprehensive analysis of the petrology and mineralogy of the volcanic glass, coupled with multiple thermodynamic modeling techniques. Through the investigation, we aim to shed light on the petrological characteristics and evolutionary history of the glass. The results indicate that the primitive magma of the glass was created at 1398–1436°C and 8.3–11.9 kbar (166–238 km) from an olivine+orthopyroxene mantle source region. Then, the magma ascended toward the surface along a non-adiabatic path with an ascent rate of ~ 40 m s^{-1} or 0.2 MPa s^{-1}. During the magma ascent, only olivine crystallized and the onset of magma eruption occurred at $\sim$ 1320–1343°C. Finally, the glass cooled rapidly on the lunar surface with a cooling rate ranging between 20 and 200 K min^{-1}. Considerable evidence from petrology, mineralogy, cooling rate, and the eruption rate of the glass beads strongly supports the occurrence of ancient explosive volcanism on the Moon.

INTRODUCTION

Early volcanic activity was widespread on the Moon and recorded by returning lunar samples (e.g., Li et al., 2021; Nicholis & Rutherford, 2009; Papike et al., 1990; Zellner et al., 2009) and lunar meteorites (e.g., Demidova et al., 2003; Fagan et al., 2002; Zeng et al., 2021). Lunar pyroclastic deposits are low-albedo, mantling deposits that were emplaced by explosive volcanism ranging from 2.3 to 3.7 Ga, thus could shed light on the nature of the early volcanism on the Moon (e.g., Bennett & Bell, 2023; Heiken et al., 1974; Hiesinger et al., 2011). Remote sensing data have identified over 100 lunar pyroclastic deposits, often located on the edges of the maria and overlapping onto adjacent highland regions (e.g., Bennett & Bell, 2023; Lucey et al., 2006). The Apollo missions have returned lunar pyroclastic deposits, known as "picritic glass beads", which serve as ground truth for remote sensing observations. The composition of picritic glass beads ranges from low-Ti (<2 wt% TiO_2) to intermediate-Ti (3–7 wt% TiO_2) to high-Ti (8–16 wt% TiO_2), implying chemically distinct source regions within the upper lunar mantle (e.g., Delano, 1986; Hess & Parmentier, 1995; Shearer et al., 2006).

The multiple saturation point (MSP) of olivine and pyroxene is commonly used as an indicator of the source regions of primary magmas on the Moon (e.g., Haupt et al., 2023; Shearer et al., 2006; Su et al., 2022). High-pressure experiments on Apollo picritic glass compositions have shown that the MSPs of olivine and orthopyroxene occur at 1.5–2.5 GPa and 1430–1560°C, respectively (Shearer et al., 2006). This suggests that the Apollo picritic glass could represent partial melts derived from olivine+pyroxene±garnet source regions at depths of 300–500 km (BVSP, 1981; Delano & Livi, 1981; Green et al., 1974; Grove & Krawczynski, 2009; Walker et al., 1975). Therefore, the primitive composition of picritic glass provides valuable constraints on the petrogenesis of lunar pyroclastic deposits and helps to unravel the compositional heterogeneity and early thermal state of the lunar mantle (Brown & Grove, 2015; Delano, 1986; Elkins-Tanton et al., 2000, 2003; Keske et al., 2020; Shearer & Papike, 1993).

Compared to crystal-free glass, phenocrysts within picritic glass beads offer additional insights into their petrogenesis and the nature of their source regions. For example, the compositions, model abundances, and the number of crystalline phases are directly linked to the evolutionary processes and thermal dynamics within the magma system (Haggerty, 1974; Heiken et al., 1974; Weitz et al., 1999). The chemical zonings of minerals can be used to constrain the cooling rate and burial depth (e.g., Arndt & von Engelhardt, 1987; McCallum & O'Brien, 1996; Richter et al., 2021). However, there is a scarcity of phenocrysts in the picritic glass beads from the Apollo collections, and detailed reports on olivine-in-glass are limited to Apollo 17 orange glass (Arndt & von Engelhardt, 1987; BVSP, 1981; Haggerty, 1974; Heiken et al., 1974). This hinders our understanding of the petrogenesis and provenance of lunar pyroclastic deposits from a mineralogical perspective. Furthermore, compositional studies using near-infrared data have revealed that lunar pyroclastic deposits exhibit a wide range from crystalline to glass-rich and are widespread on the Moon (Bennett & Bell, 2023). Unfortunately, apart from the samples returned by the Apollo missions, no pyroclastic deposit has been reported in detail, although a few have been found in lunar meteorites (e.g., NWA 11962, Bechtold et al., 2022).

In this study, we present a detailed petrology and mineralogy analysis of picritic glass beads in the newly discovered lunar regolith breccia meteorite, NWA 11801. This is the first reported instance of a pyroclastic deposit in meteorites, potentially contributing to the diversity of rock types found on the Moon. The glass beads within NWA 11801 contain olivine phenocrysts with chemical zoning, providing new constraints on early explosive volcanism on the Moon. Our investigation aims to quantify the cooling history of these volcanic glass beads during magma ascent and eruption through microscopic analysis and thermodynamic modeling, shedding new light on the source region of pyroclastic deposits on the Moon.

METHODS

A conventional polished thin section (0.03 mm) was coated with carbon and then analyzed using multiple analytical techniques. Backscattered electron (BSE) images and x-ray maps were collected by a Zeiss ΣIGMA field emission scanning electron microscope (FE-SEM) in the mode with an accelerating voltage of 15 kV at the Guilin University of Technology. The quantitative major and minor element compositions of glass beads and olivine were obtained by the JEOL JXA-8230 electron probe microanalyzer (EPMA) at the same university. The primary EPMA method is described in detail by Zeng et al. (2019). This instrument was operated at an accelerating voltage of 15 kV with an electron beam current of 20 nA. A focused beam of <1 μm was used for olivine, while a defocused beam of 3–5 μm was used for glass. Natural and synthetic crystals are used as standards for the analyses, and ZAF correction was applied to all analyses. The minerals standard (CAS) was used for the quantitative analysis of olivine phenocrysts: olivine was employed for Si, Fe, and Mg; rutile for Ti; albite for Al and Na; Cr metal for Cr; MnO for Mn; wollastonite for Ca; and phlogopite for K. The following standards were used for the quantitative analysis of glass:

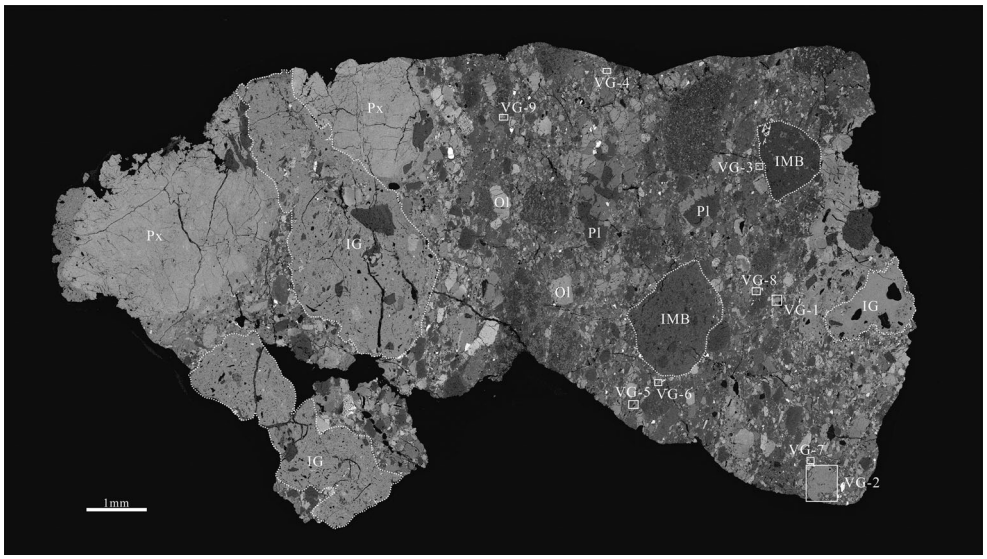

FIGURE 1. Backscattered electron (BSE) mosaic image of thin section NWA 11801. IG, impact glass; IMB, impact melt breccia; Ol, olivine; Pl, plagioclase; Px, pyroxene; VG, volcanic glass.

basalt glass was employed for Si, Al, Fe, Mg, and Ca; rutile for Ti; chromite for Cr; MnO for Mn; albite for Na; phlogopite for K; elemental nickel for Ni; apatite for P; $Ca_2(VO_4)_2$ for V; and pyrite for S. The typical detection limits of the oxides were 0.01 wt% for SiO_2, Al_2O_3, MgO, and CaO; 0.015 wt% for Cr_2O_3, FeO, MnO, Na_2O, K_2O, and NiO; and 0.02 wt% for TiO_2, P_2O_5, and SO_3.

Raman spectra of lattice olivine in the sample were collected using a Renishaw inVia Raman spectrometer system at Guilin University of Technology, equipped with an AR^+ laser (at 514 nm) (Chou & Wang, 2017). A silicon wafer ($520.7 \pm 0.5\ cm^{-1}$) was used for calibration. The power of the laser had to be low enough to avoid heating, degradation, and burning of the sample. The measurement used 0.5 mW and a spot size of 1 μm. The microscope imaged the area with 100× magnification with five scans. Finally, the OriginPro 95 Software was used to subtract baselines, find peaks, and fit peaks for the acquired Raman data.

RESULTS

The Lunar meteorite NWA 11801 is a lunar regolith breccia, composed of mineral fragments, lithic clasts, and glass components. The mineral fragments and lithic clasts primarily comprise plagioclase, pyroxene, olivine, and impact melt breccias (Figure 1). Two types of glass can be identified in the sample: One is large (many of them >1 mm in size), ragged, and compositionally heterogeneous impact glass (IG, Figure 1), and the other is small (~ 50 μm in size), devitrified, compositionally homogeneous volcanic glass (VG, Figures 1 and 2). Nine pieces of volcanic glass were found in the thin section (VG-1–VG-9, Figure 1).

The volcanic glass shows distinctive structural features (Figure 2). It displays a range of shapes, including spheroid (Figure 2c,d,h), ovoid-like sphere (Figure 2a,b), and irregular forms (Figure 2e–g,i). The volcanic glass exhibits varying degrees of devitrification texture, with VG-8 and VG-9 completely devitrified (Figure 2h,i), while others appear to have undergone partial devitrification (Figure 2a–g). Only one (VG-2) contains crystalline olivine that does not result from devitrification (Figure 2b), corresponding to the "daughter" olivine grains shown in Figure 3. Vesicles are pervasive in VG-3, VG-5, and VG-7, while less abundant in VG-6 and VG-9 (Figure 2). Others (VG-1, VG-2, VG-4, and VG-8) are devoid of vesicles (Figure 2a,b,d,h). The occurrence of vesicles and pronounced irregular morphology of VG-3, VG-5, and VG-7 suggest that some of the volcanic glass samples have been affected by impact reheating and possibly originate from an impact melt derived from a predominately volcanic glass deposit. Chemically, the volcanic glass has elemental ratios of MgO/Al_2O_3 (1.37–1.54) and CaO/Al_2O_3 (0.94–1.10), which are typical for lunar volcanic glass beads (Table S1). Besides, the volcanic glass is characterized by low TiO_2 (0.35–0.70 wt%) and alkaline element contents (0.07–0.27 wt%) (Figure 4). The combined major element contents indicate that the bulk compositions of the volcanic glass closely resemble the very low-Ti (VLT) glass found at the Apollo 14 and Apollo 17 landing sites (Figure 4).

Two types of olivine are present in the olivine-bearing volcanic glass VG-2. The first type is referred to

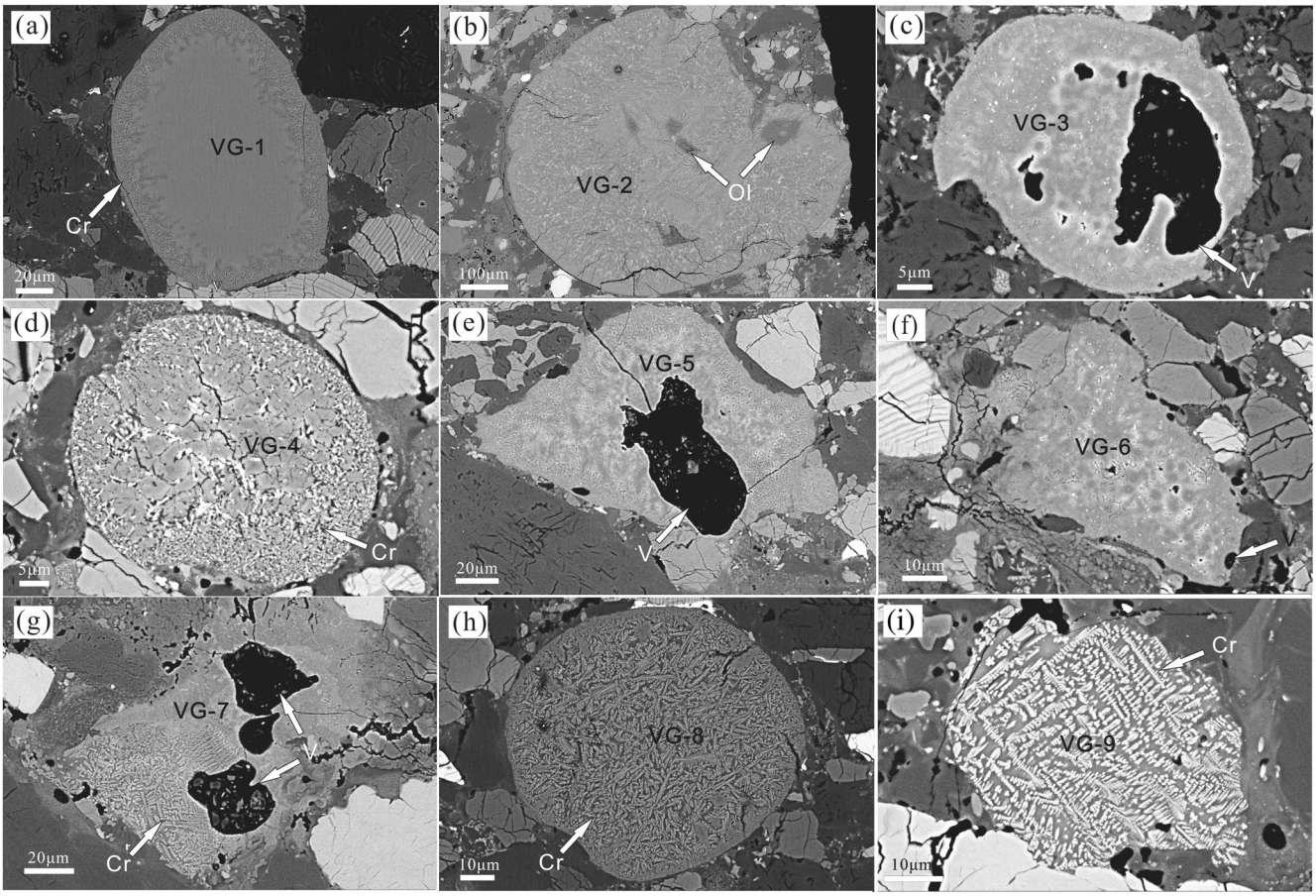

FIGURE 2. Backscattered electron images of volcanic glass (a–i). Cr, crystallite; V, vesicle; VG, volcanic glass.

as polyhedral olivine, characterized by a euhedral morphology with sizes ranging from 10 × 20 to 45 × 80 μm (Figure 3). These olivine grains display chemical zoning, with homogeneous cores ($Fo_{76.0–77.8}$) surrounded by thin, bright rims ($Fo_{68.8–75.8}$) (Table S2). Using the olivine-liquid Fe-Mg exchange coefficient of 0.33 ± 0.03 (Longhi et al., 1978), the cores of olivine are generally in equilibrium with the bulk glass (Mg#58.2) (Table S1). The second type is referred to as lattice olivine, which is smaller in size (~ 1 μm in width) and exhibits a feathery appearance (Figure 3). These lattice olivine crystals are pervasively distributed within the devitrified glass (Figure 3). Raman spectroscopy analysis confirms their identity as olivine, as indicated by peak positions at ~ 818–820 and 844–849 cm^{-1} (Mouri & Enami, 2008) (Figure 5). Due to their minute size, it is not feasible to accurately determine the composition of the lattice olivine through EPMA data.

Melt inclusions are present in each olivine grain, ranging in size from 1 × 1 to 10 × 11 μm. They are glassy and have undergone devitrification (Figure 3). The melt inclusions can be classified as either closed (Figure 3a–d) or fractured (Figure 3e,f). Their chemical compositions are distinct from those of the host glass, mainly by lower Mg# (34.1–49.3) and higher alkaline element contents (0.07–0.17 wt% for Na_2O and 0.02–0.06 wt% for K_2O) (Table S3).

DISCUSSION

Glass Beads in NWA 11801: Impact or Volcanic?

According to the origin, two types of glass samples have been documented thus far: lunar impact glass and volcanic (pyroclastic) glass. Previous studies on lunar samples returned by the Apollo missions and lunar meteorites have established criteria for distinguishing between lunar volcanic glass and impact glass (Delano, 1986; Naney et al., 1976; Zeng et al., 2019, 2020). Overall, the lunar volcanic glass samples are bead-like, devoid of schlieren and exotic inclusions, with higher MgO/Al_2O_3 (>1.25) and CaO/Al_2O_3 (>0.75) (Delano, 1986; Naney et al., 1976) ratios. The volcanic glass in NWA 11801 displays various shapes, including spheroid (Figure 2c,d,h), ovoid-like sphere (Figure 2a,b), and irregular shapes (Figure 2e–g,i). These morphologies are

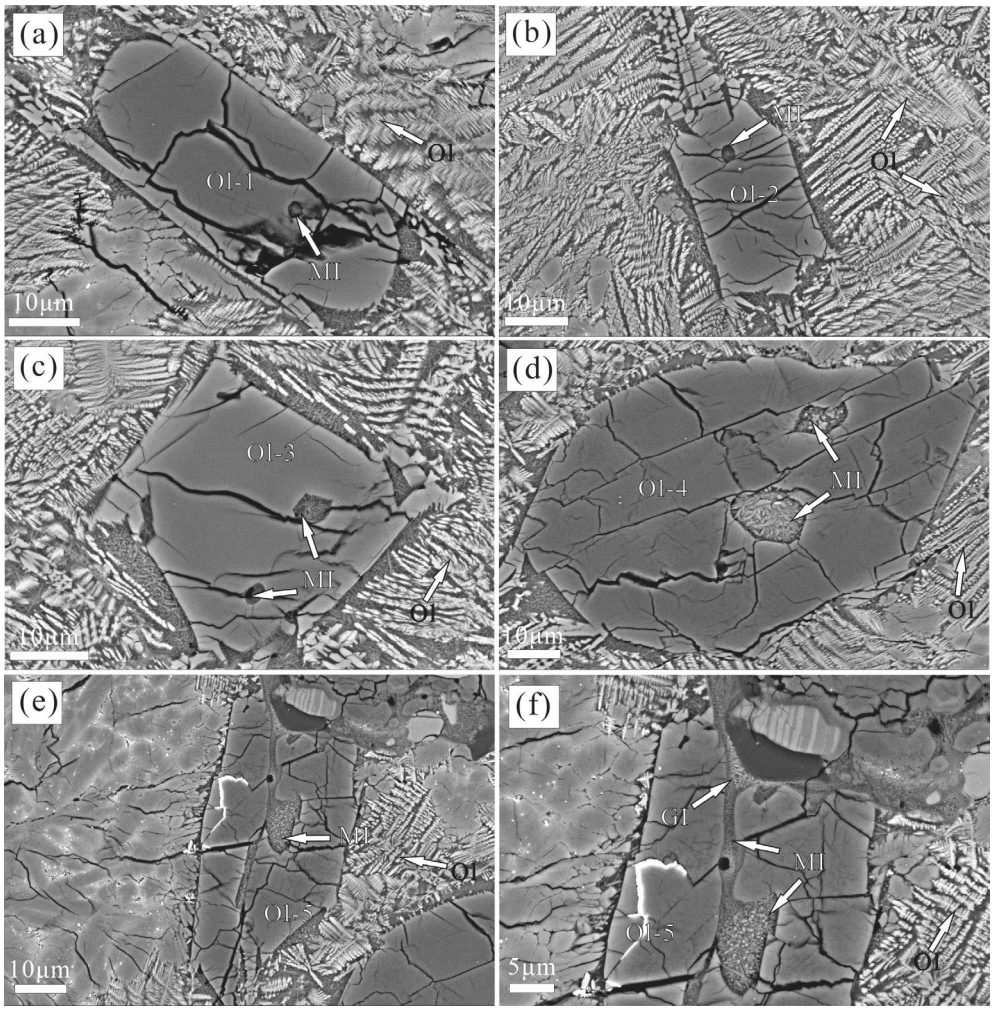

FIGURE 3. Backscattered electron images of volcanic glass and daughter olivine grains. (a–e) BSE image of olivine within the volcanic glass. (f) A zoom-in image of (e), showing melt inclusions. Ol, olivine; MI, melt inclusion; VG, volcanic glass.

consistent with the shape of volcanic glass previously found in Apollo collections and lunar meteorites (Delano, 1979; Zeng et al., 2019, 2020). Furthermore, the absence of schlieren in the glass beads is consistent with the characteristics of volcanic glass beads (Delano, 1986). In addition, both MgO/Al_2O_3 (1.37–1.63) and CaO/Al_2O_3 (0.94–1.10) ratios fall within the compositional range of volcanic pyroclastic glass (Figure 6), indicative of a volcanic origin (Delano, 1986; Naney et al., 1976). Therefore, we conclude that the glass beads found in NWA 11801 are more likely to be of volcanic origin rather than impact glass.

Melt Inclusions in Olivine: Indicative of Olivine Crystallization

Melt inclusions of both closed and fractured are present (Figure 3). These melt inclusions are characterized by a monophase composition, with olivine being the sole crystallizing mineral observed along their boundaries. Chemically, the fractured melt inclusions exhibit a more scattered distribution compared to the closed melt inclusions. This scattering is probably due to elemental diffusion and contamination processes. In general, the melt inclusions display lower Mg# and higher concentrations of Si, Ca, Al, Ti, Cr, Na, and K (Figure 7). These elemental contents show notable linear correlations with those of host glass beads in the Harker diagrams (Figure 7).

To investigate the controlling factors of these linear correlations, we modeled the evolution trend of an initial melt with a composition similar to that of the average host glass beads. This simulation was performed using rhyolite-MELTS, considering both equilibrium and fractional crystallization modes (Ghiorso & Gualda, 2015; Gualda et al., 2012). The modeling results indicate that after

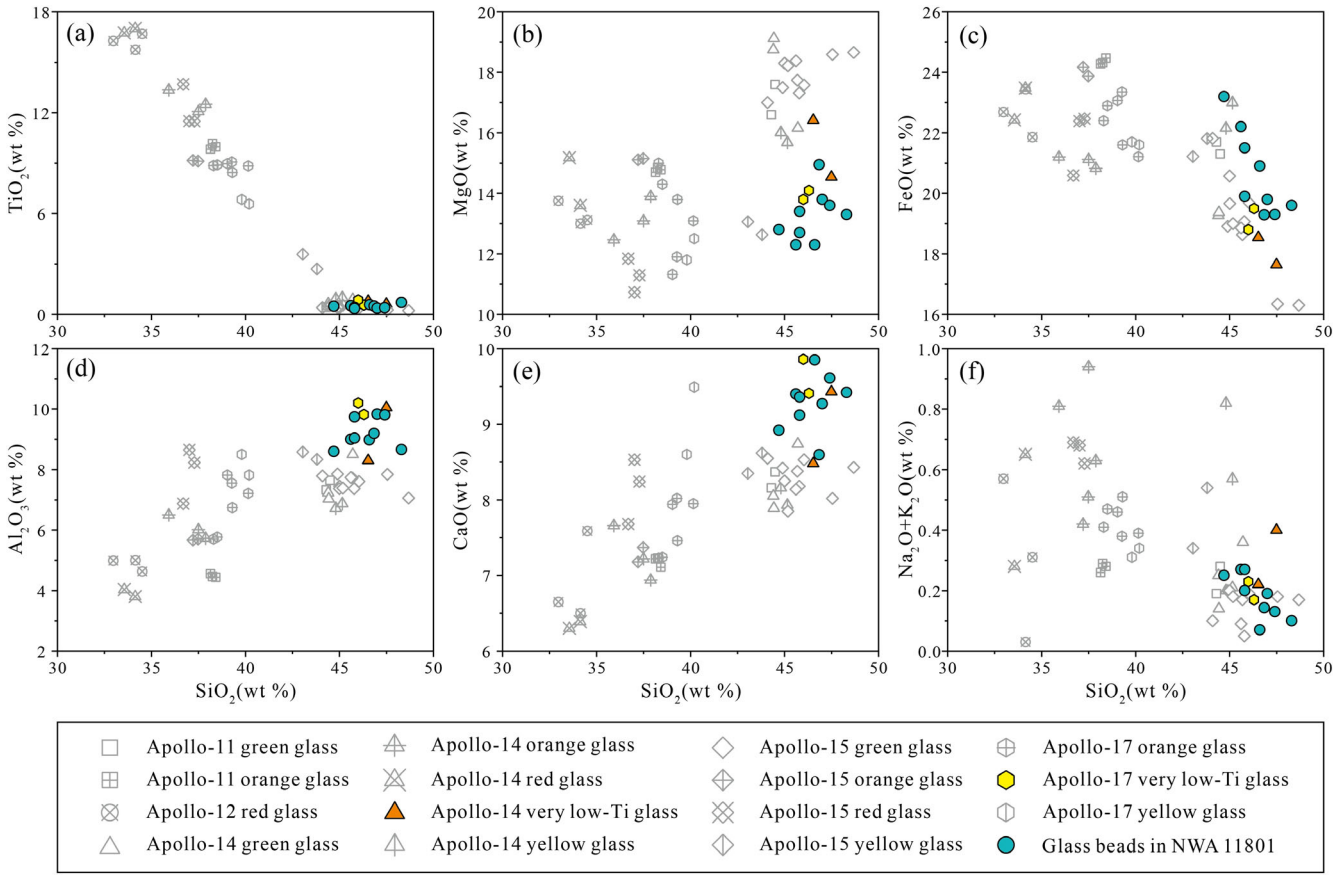

FIGURE 4. Bulk chemical compositions of volcanic glass in NWA 11801, compared with the bulk compositions of other types of volcanic glass in Apollo collections (see supplemental data for Jolliff et al., 2006). (a) SiO_2 versus TiO_2; (b) SiO_2 versus MgO; (c) SiO_2 versus FeO; (d) SiO_2 versus Al_2O_3; (e) SiO_2 versus CaO; (f) SiO_2 versus Na_2O+K_2O. (Color figure can be viewed at wileyonlinelibrary.com)

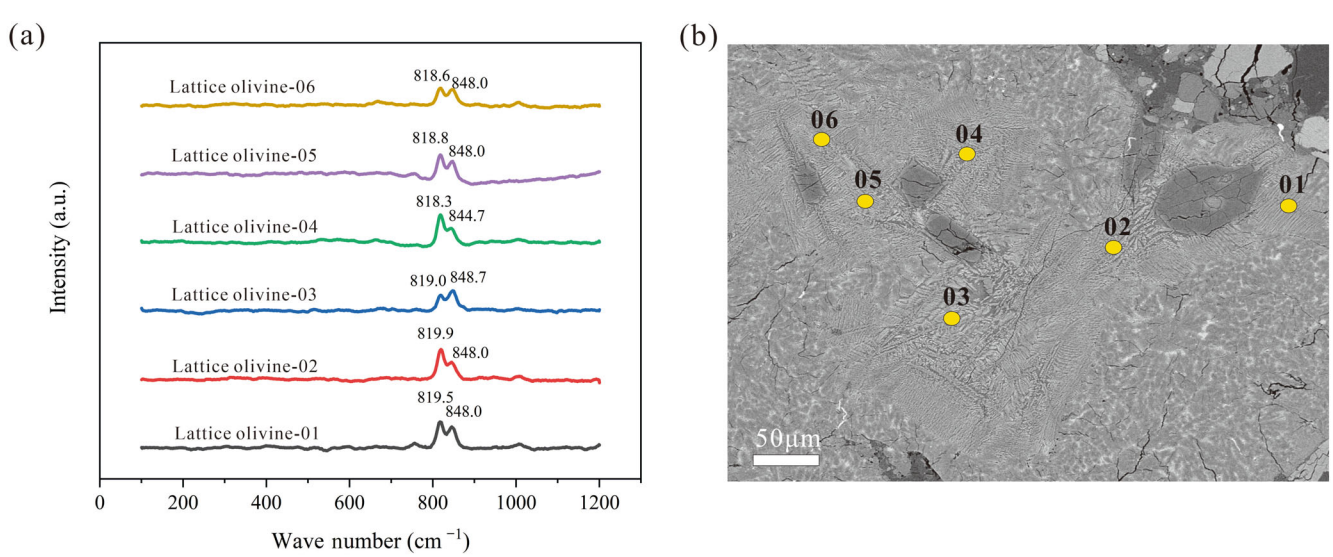

FIGURE 5. Raman spectra of lattice olivine in VG-2. (a) Raman spectra of lattice olivine-01–06, after baseline correction. (b) The positions of lattice olivine-01-06. (Color figure can be viewed at wileyonlinelibrary.com)

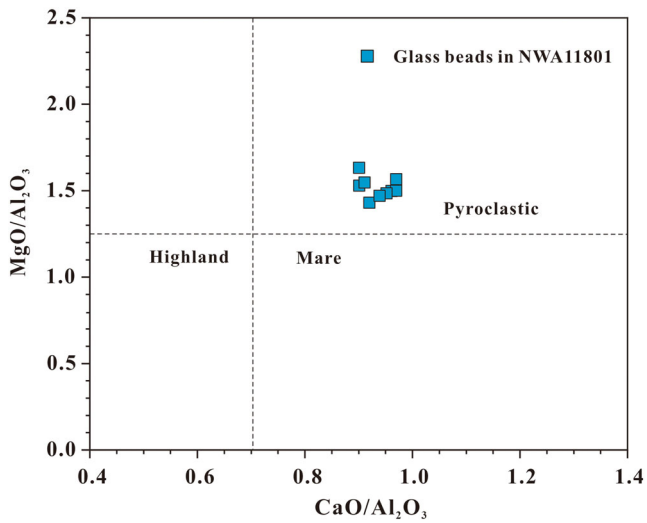

FIGURE 6. The bulk MgO/Al_2O_3 versus CaO/Al_2O_3 (in weight ratios) diagram of glass beads in NWA 11801. The horizontal and vertical dashed lines highlight the MgO/Al_2O_3 ratio of 1.25 and CaO/Al_2O_3 ratio of 0.75, respectively (following Zeng et al., 2019), indicating a pyroclastic origin for the glass beads (blue squares) in NWA 11801. (Color figure can be viewed at wileyonlinelibrary.com)

~ 40 wt% of olivine monophase crystallization, the composition of host glass beads can evolve to that of melt inclusions, regardless of their specific textures (Figure 7).

However, the estimated contents of alkaline elements in the melt inclusions are remarkably lower than the measured values (Figure 7). This discrepancy could potentially be attributed to the boundary layer effect, as suggested by Lasaga (1981) and Kuzmin and Sobolev (2003). Boundary layers may form at the interfaces between growing crystals and the surrounding melt, leading to the trapped melt inclusions enriched in incompatible elements (e.g., Chang & Audétat, 2021). Another possible explanation is that the mantle source of the glass beads might have undergone metasomatism, similar to the case presumed in nakhlites (Day et al., 2018; Goodrich et al., 2013), resulting in an excessive enrichment of alkaline elements in olivine-hosted melt inclusions. However, both the boundary layer effect and mantle metasomatism lack direct evidence, making it difficult to quantitatively evaluate their likelihood. Nonetheless, the modeled trends in Figure 7 are mostly consistent with the equilibrium crystallization of olivine in a closed system.

Olivine as a Proxy of Melt Ascent and Eruption

The picritic melt forming the pyroclasts was transported from sources at depths of 250–600 km to the lunar surface on time scales of hours to days (e.g., Grove & Krawczynski, 2009). Importantly, there was no significant chemical interaction observed between the transported melt and the surrounding rocks during its ascent (Wilson & Head, 2017, 2018). As the melt ascended, olivine was the first mineral to precipitate and continued crystallizing from the deep interior to the surface of the Moon (Howarth & Gross, 2019). Understanding the properties of olivine can contribute to gaining better comprehension of the formation process of the glass beads. The following sections show how the volcanic glass in this sample supports these fundamental characteristics of lunar volcanic glasses.

Melt Ascent from the Lunar Interior

In the Moon's deep interior, the melt comprising the volcanic glass beads ascends along a specific pressure–temperature (P–T) path through the mantle's wall rocks, driven by buoyancy force. The P–T path of the ascending melt was determined by using the Si-activity liquid thermobarometer (Lee et al., 2009), based on the bulk compositions of glass beads. Our results give temperatures of 1400–1450°C and pressures of 7–13 GPa. The latter pressure range corresponds to depths of 140–260 km. All the bulk compositions of the glass beads plotted in the P–T space exhibit excellent alignment, forming a linear relationship described by the equation T (°C) = $0.4822D + 1320$ (D in km; 1 kbar = 20 km on the Moon). This equation reveals a thermal gradient $\frac{\partial T}{\partial D}$ of 0.48°C km^{-1} for the ascending melt, which exceeds the range of the lunar mantle's adiabatic gradient (0.045–0.17°C km^{-1}, Johnson et al., 2018; Walker et al., 1980) and indicates heat loss during ascent. The linear fit predicts an eruption temperature of ~ 1320°C, consistent with the estimation based on bulk-rock MgO content (1343°C, using the equation T (in °C) = 26.3 × MgO + 994.4 (Putirka, 2008)). These findings indicate that the melt of glass beads in NWA 11801 ascended through the Moon's interior in a non-adiabatic (anisentropic) manner from depths of ~ 260 km.

The phase equilibrium relations in P–T space (Figure 8) are estimated using GeoPS program (Xiang & Connolly, 2021). This program employs phase equilibrium calculations based on Gibbs energy minimization. The thermodynamic database ds633 of Holland et al. (2018) and the chemical system of NCKFMASTCr (Na_2O-CaO-K_2O-FeO-MgO-Al_2O_3-SiO_2-TiO_2-Cr_2O_3) were used, consistent with an igneous origin, low oxygen fugacity, and the absence of hydrous minerals. The starting composition for the calculation is the average bulk composition of volcanic glass beads. The calculation results indicate that olivine is the liquidus phase, and the monophase crystallization of olivine during magma ascent is consistent with the petrological observations and evolution trends of the melt inclusions (see "Melt Inclusions in Olivine: Indicative of Olivine Crystallization" Section). Along the magma ascent path

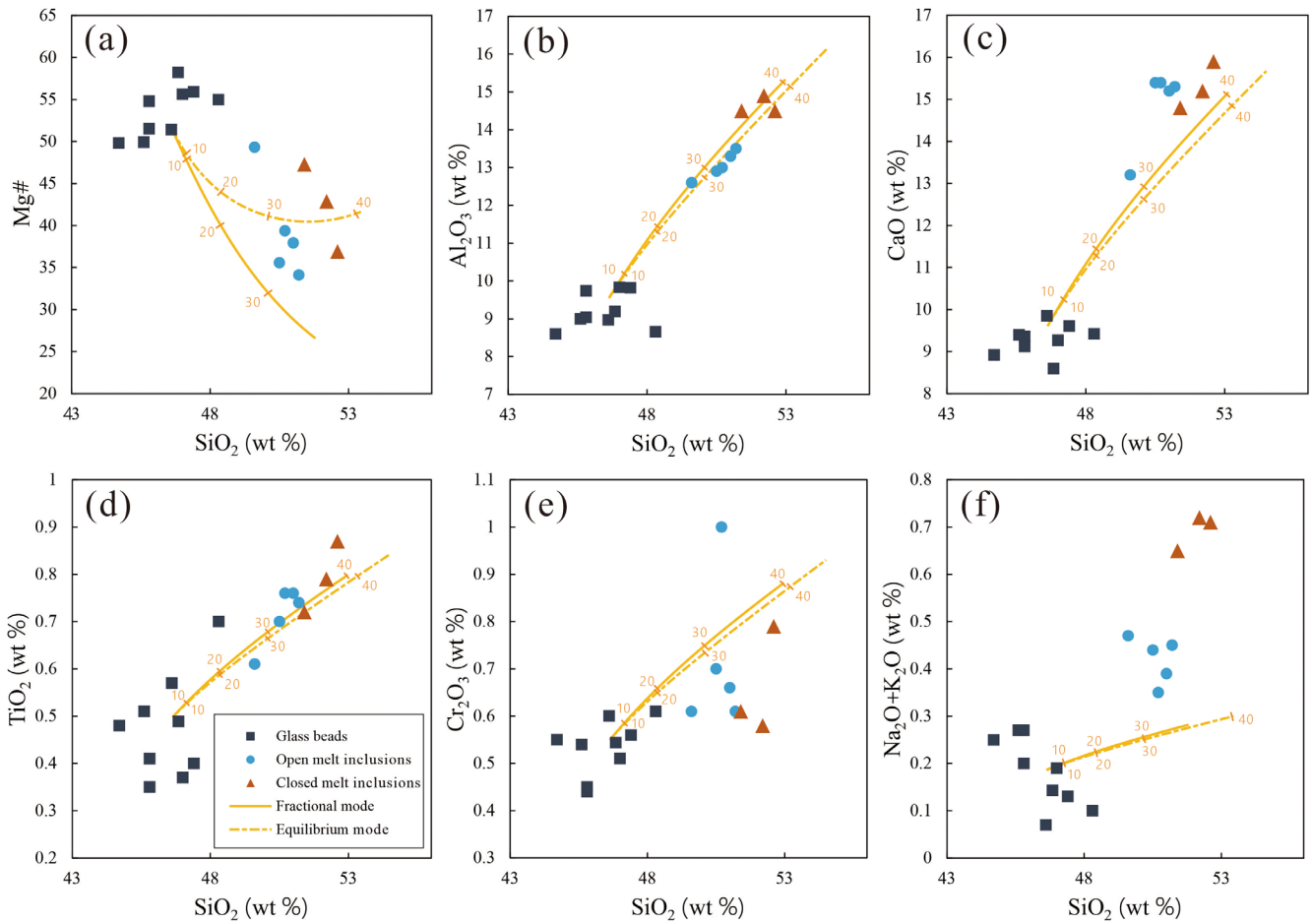

FIGURE 7. Elemental compositions of the studied glass beads and melt inclusions. (a) SiO_2 versus Mg#; (b) SiO_2 versus Al_2O_3; (c) SiO_2 versus CaO; (d) SiO_2 versus TiO_2; (e) SiO_2 versus Cr_2O_3; (f) SiO_2 versus Na_2O+K_2O. Yellow numbers in each panel denote the crystallinity (in wt%) of the magma. (Color figure can be viewed at wileyonlinelibrary.com)

determined by the liquid thermobarometer, the onset of olivine crystallization occurs at ~ 1400°C and ~ 11 kbar (corresponding to a depth of ~ 220 km) (Figure 8).

In experimental glass samples, the olivine crystallization rate typically falls within the range of 10^{-8}–10^{-9} m s^{-1} (Mollo & Hammer, 2017). With an average crystallization rate of 5×10^{-9} m s^{-1} and a radius of the largest olivine crystal (30 μm), the time span of magma ascent is constrained to be ~ 6000 s. The estimated magma ascent rate is thus ~ 40 m s^{-1} or 0.2 MPa s^{-1} (from ~ 220 km depth to the surface), in agreement with previous estimates for lunar explosive volcanism (typically 20–30 m s^{-1}, some reaching 220 m s^{-1}) (Wilson & Head, 2018). It should be noted that the velocity calculations based on the olivine crystallization rate may oversimplify the magma ascent process. Nevertheless, providing an estimate on the order of magnitude of the magma rising rate indicates that the magma may have a high velocity during its ascent in the magma conduit.

Melt Eruption on the Lunar Surface

The olivine crystals within the glass beads exhibit enrichments of Fe, Ca, and Al in the rim regions (Table S2). As Ca and Al are incompatible in olivine, this observation indicates a disequilibrium crystal growth process due to fast cooling (Donaldson, 1976; Faure et al., 2003). Under natural crystallization conditions, growth at large undercooling can lead to the formation of disequilibrium olivine. In this case, olivine growth is dominantly controlled by elemental diffusion rather than the crystal–melt interface (Mollo & Hammer, 2017; Montazerian & Zanotto, 2022 and references therein). Therefore, the cooling rate of the glass beads can be determined by core–rim diffusion calculations, which is crucial for understanding the eruption and final emplacement process of glass beads.

To estimate the cooling rates, Fo zoning profiles of olivine were calculated using the elemental diffusion model proposed by Costa et al. (2008). The temperature ranged

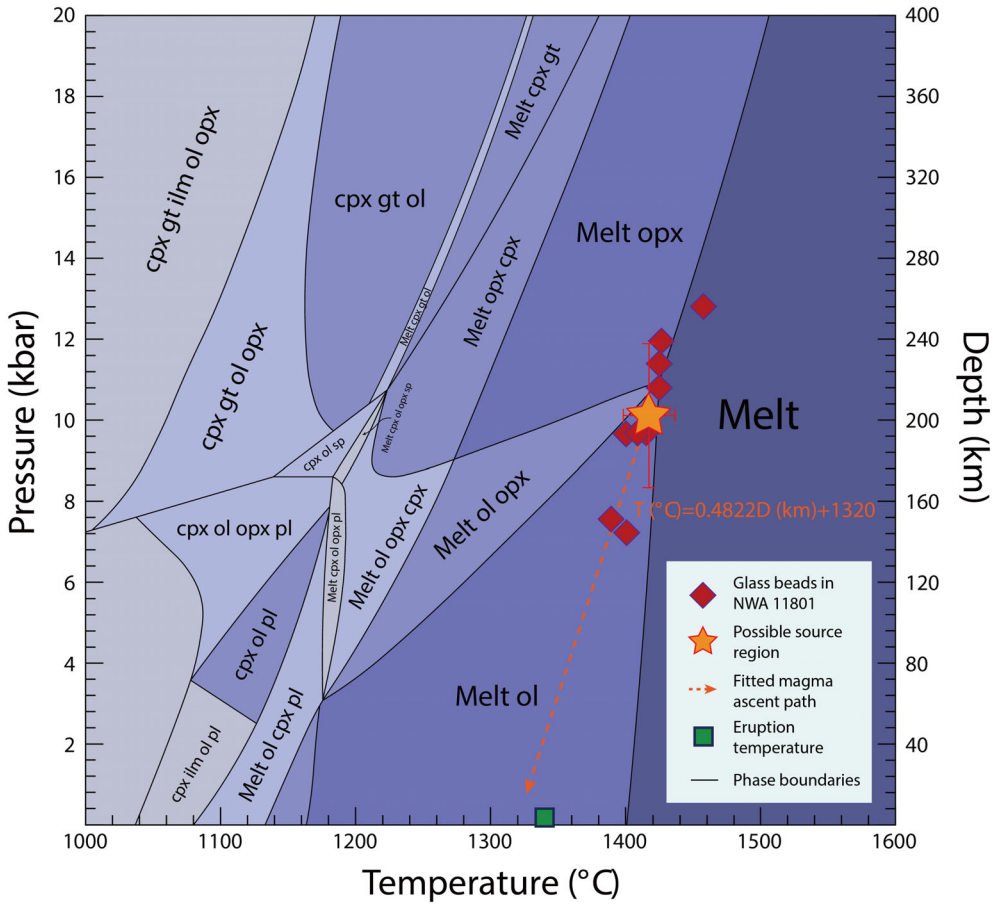

FIGURE 8. Isochemical pressure–temperature phase diagrams (pseudosections) in the NCKFMASTCr (Na_2O-CaO-K_2O-FeO-MgO-Al_2O_3-SiO_2-TiO_2-Cr_2O_3) system for the starting composition of average bulk glass beads, showing the calculated stability of equilibrium assemblages. The P–Ts of glass beads in NWA 11801 calculated by Lee et al. (2009) are shown by red diamonds, and the orange arrow indicates the fitted magma ascent path. The phase boundaries are drawn by GeoPS program (Xiang & Connolly, 2021). Mineral abbreviations (after Whitney & Evans, 2010): cpx, clinopyroxene; gt, garnet; ilm, ilmenite; ol, olivine; opx, orthopyroxene; pl, plagioclase; sp, spinel. (Color figure can be viewed at wileyonlinelibrary.com)

from 1400 to 700°C as suggested by Jurewicz and Watson (1988), and a homogeneous initial composition for each olivine crystal was used. The Fe-Mg diffusion coefficient of olivine from Misener (1974) was employed in the calculations.

The observed and calculated zoning profiles are shown in Figure 9. The olivine zoning profiles align best with cooling rates of 20–200 K min^{-1}. This profile is consistent with cooling rate estimates for Apollo 17 orange glass beads obtained through heat capacity constraints (101 K min^{-1}, Hui et al., 2018). Slight variations in cooling rates among different olivine crystals may be attributed to the different orientations of the crystals during sampling.

The occurrence of lattice olivine also suggests a cooling rate of $\sim$40–50 K min^{-1}, as constrained by crystallization experiments on Apollo-15 glass beads (Arndt et al., 1984). These estimated cooling rates are consistent with the simple ballistic eruption model for lunar pyroclastic eruptions, which determined cooling rates of glass beads during flight along ballistic trajectories exceeding 180 K min^{-1} (Renggli et al., 2017). These results indicate that the olivine crystals completed their crystallization and cooled rapidly upon reaching the chilling lunar surface. This rapid cooling likely occurred during their flight in the lunar atmospheric environment (Renggli et al., 2017).

The Source Region of Glass Beads in NWA 11801

Compared to other picritic glass beads, the glass beads examined in this study have higher SiO_2 contents and lower Mg# (Figure 4). Besides, the olivine present in these beads occurs exclusively as a primary phase with a core Fo range of 76–78, which is significantly lower than the olivine phenocrysts found in Apollo-17 orange glass

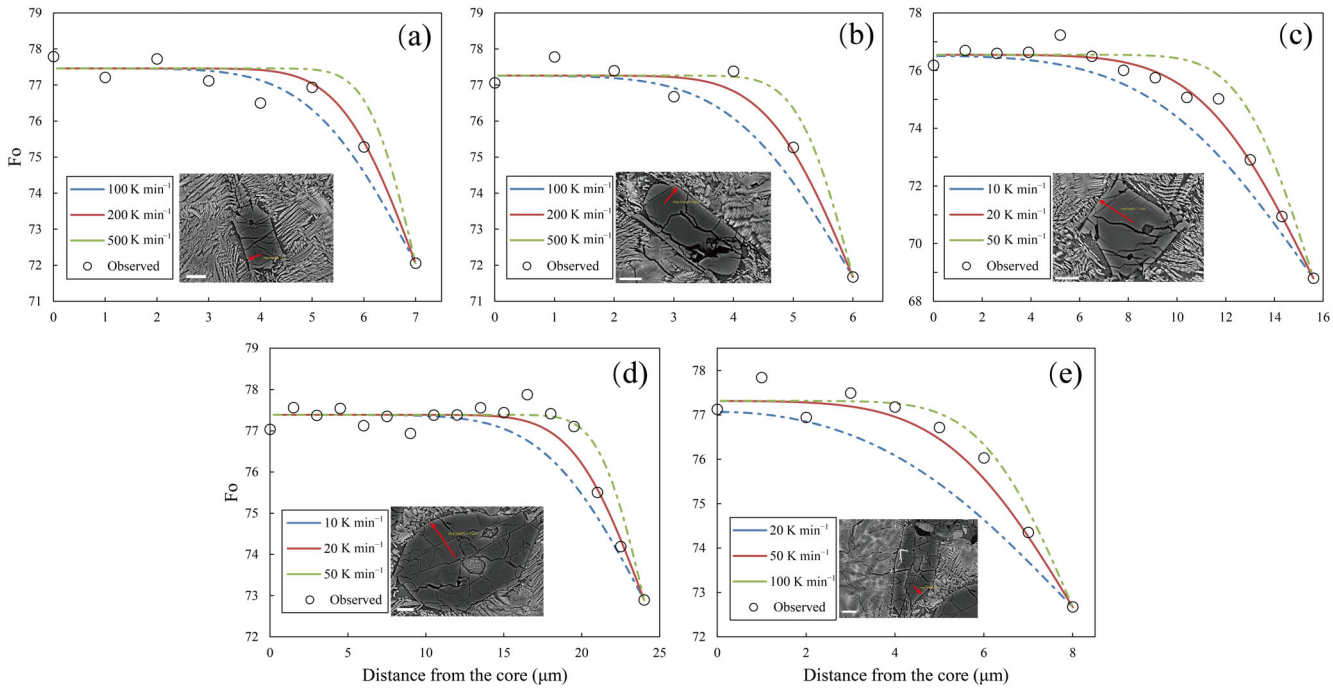

FIGURE 9. Calculated cooling rates of olivines in NWA 11801 and the original Fo zoning profiles (a–e). Observed (hollow circles) and calculated diffusion profiles in different cooling rates (colored curves) are shown together. (Color figure can be viewed at wileyonlinelibrary.com)

(Fo80-82, e.g., Heiken et al., 1974), as well as the cumulate olivine in the lunar mantle (Fo ~ 81.5, Kuskov et al., 2019). Based on the assumption that picritic glass represents primary magma, these observations suggest the possibility that the mantle source region for these beads has higher SiO_2 content and lower Mg# compared to the source regions of Apollo glass beads. In this scenario, the higher SiO_2 content likely signifies a greater amount of pyroxene in the source region, while the lower Mg# implies a chemically more evolved source region compared to Apollo glass beads. The equilibrium P–Ts of the picritic glass beads thus provide insights into the P–T condition of the source region, which is 1417 ± 19°C and 10.1 ± 1.8 kbar (Figure 8), corresponding to a depth range of 166–238 km in the lunar mantle. It is worth noting that the VLT Apollo-14 and Apollo-17 glass beads are multiply saturated with olivine and orthopyroxene at much higher P–T conditions (1480–1520°C and 16–20 kbar, equivalent to 320–400 km) (Chen et al., 1982a, 1982b). Therefore, it is unlikely that the source region of the glass beads in NWA 11801 is the same as that of the VLT Apollo-14 and Apollo-17 glass beads, despite their similarities in bulk compositions (Figure 4).

Alternatively, we also explore the possibility that the picritic glass in NWA 11801 may not represent primary magma. In this scenario, the primary magma composition can be reconstructed by adding fractionated olivine to the bulk compositions of picritic glass until the magma reaches equilibrium with cumulate olivine (Fo ~ 81.5) in the lunar mantle (Kuskov et al., 2019). The reconstruction process is conducted using PRIMELT3, which is a widely used method for calculating primary magma compositions based on natural bulk compositions (Herzberg & Asimow, 2015). After adding ~9 wt% of fractionated olivine, the composition (in wt%) of the reconstructed primary magma is as follows: SiO_2 45.7, TiO_2 0.44, Al_2O_3 8.41, Cr_2O_3 0.5, FeO 20.43, MnO 0.24, MgO 15.43, CaO 8.48, Na_2O 0.15, and K_2O 0.02. Using the Si-activity liquid thermobarometer proposed by Lee et al. (2009), the calculated P–T condition of the primary melt is 1495°C and 16.7 kbar (corresponding to a depth of 334 km). The result is therefore consistent with those of picritic glass beads collected by Apollo missions (250–500 km) (Grove & Krawczynski, 2009) and the multiple saturation experiments of mare basalts (Lee et al., 2009 and references therein).

The latter scenario suggests the early fractionation of high Mg# olivine in the formation of glass beads. However, MELTS modeling results tend to indicate an equilibrium crystallization of olivine, as fractional crystallization would lead to a residual melt with a much lower Mg# than what is observed (Figure 7a). Furthermore, olivine with higher Mg# (Fo > 80) is absent in the glass beads, which contradicts the assumption that the glass beads evolved from a more primary magma.

Therefore, it is more likely that the picritic glass represents primary magma. As discussed above, the source region for these glass beads is likely richer in SiO_2, more chemically evolved, and located at shallower depths (166–238 km) compared to the source regions of Apollo glass beads. The enrichment in SiO_2 content in the glass beads likely indicates a pyroxene-rich mantle source, as pyroxene contains more SiO_2 than olivine. Additionally, the presence of orthopyroxene at the P–T condition of the source region supports the notion of an orthopyroxene-dominated source region, as shown by the phase diagram (Figure 8). Therefore, it is likely that the source region of the picritic glass in NWA 11801 is composed predominantly of olivine and orthopyroxene.

Considering that Al- and Ca-rich phases had been extracted in the lunar crust during the stage of the lunar magma ocean (Rutherford et al., 2017 and references therein), the significant phases remaining in the source regions were olivine and orthopyroxene (Shearer et al., 2006). In addition, orthopyroxene in the deep mantle can also sequester significant amounts of Al, leading to Al depletion in the source region rocks, which is the case observed in bulk glass data (Figure 4). Therefore, we conclude that the picritic glass in NWA 11801 originated from a depleted mantle source predominantly composed of olivine and orthopyroxene. The source region of the picritic glass in NWA 11801 is located at shallower depths than those of Apollo picritic glass, which typically have depths of 300–500 km (e.g. Grove & Krawczynski, 2009; Shearer et al., 2006).

Implications for Explosive Volcanism on the Moon

Explosive volcanism occurs when subsurface magma becomes fragmented because of the expansion of dissolved gas (e.g., Rothery et al., 2022; Wilson & Head, 1981, 1983). In the case of the Moon, the atmospheric pressure is essentially zero, and the gravitational acceleration (1.63 m s^{-2}) is much lower than on Earth. Therefore, even minimal amounts of volatiles should guarantee explosive activity (Rothery et al., 2022 and references therein). Due to the extremely low oxygen fugacity (IW-1 or lower, e.g., Wieczorek et al., 2006), the species of volatiles on the Moon is dominantly several hundred ppm of CO, H_2, and S (Head & Wilson, 2017; McCubbin et al., 2015; Wilson & Head, 2003, 2017, 2018), which would degas at the subsurface depth (<2.3 kbar or <46 km, e.g., Rothery et al., 2022).

In the deep interior of the Moon, however, the driving force of magma ascent is the density contrast between the melt and the mantle wall rock, along with the excess pressure of the mantle source region (e.g., Gudmundsson, 2012; Head & Wilson, 2017). This integrated force propels the primary magma from the source region (at a depth of 166–238 km and a temperature of 1398–1436°C) to the shallow part, with a velocity of ~ 40 m s^{-1}. At a temperature of ~ 1400°C and a depth of ~ 220 km, olivine starts to crystallize until the final eruption occurs at temperatures of ~ 1320–1343°C.

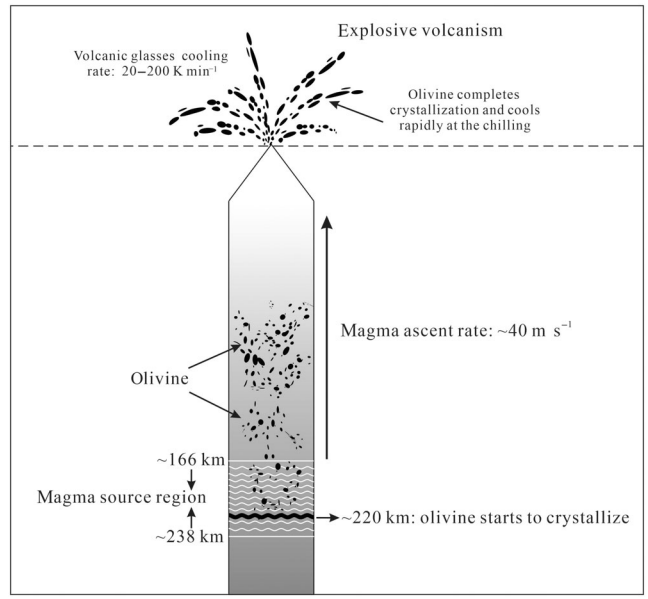

FIGURE 10. Idealized schematic diagram of the petrogenesis of volcanic glass in NWA 11801, indicating its generation, ascent, and final eruption processes on the Moon.

At the lunar surface, the absence of atmospheric pressure and the low gravitational acceleration lead to the swift expansion of the exsolved gas phases, resulting in explosive volcanism. Various lines of evidence from petrology, mineralogy, cooling rate, and eruption rate of glass beads collectively indicate the occurrence of such a cataclysmic event. First, the devitrification of glass beads and the elemental enrichment trend of olivine rims suggest disequilibrium crystallization during the final cooling of the pyroclastic glass. These processes are characteristic of typical glass textures produced by explosive volcanism (e.g. obsidian; Fink & Griffiths, 1998). Second, basic diffusion calculations indicate that the glass cooled rapidly on the lunar surface, with cooling rates ranging from 20 to 200 K min^{-1}, which is consistent with typical cooling rates during flight. Third, the calculated ascent velocity of ~ 40 m s^{-1} corresponds to a magma eruption rate of ~ 5×10^4 m^3 s^{-1} for a cylindrical magma conduit with a radius of ~20 m (Head & Wilson, 2017). This result agrees with the eruption rate estimated for lunar pyroclastic volcanism (10^4 to 10^6 m^3 s^{-1}) based on independent volcanic physics modeling methods (Head & Wilson, 2017).

Therefore, there is no doubt that the glass beads in NWA 11801 are products of ancient explosive volcanism on the Moon, depicting the process of magma eruption, as shown in Figure 10. Further investigations involving trace element and volatile species analysis should be conducted to address important remaining questions, such as the volatile contents of magma, the nature of the glass-bead source region, and the lunar mantle heterogeneity (e.g., Elardo et al., 2011; Haupt et al., 2023; Klaver et al., 2021; Morgan et al., 2021; Saal & Hauri, 2021).

CONCLUSIONS

Based on our comprehensive study, we have reached the following conclusions:

1. The present study focuses on the petrology and mineralogy of nine volcanic glass beads found in lunar meteorite NWA 11801. Among them, one glass bead contains lattice and polyhedral olivine. The bulk compositions of these glass beads exhibit similarities to the very low-Ti glass samples collected from the Apollo 14 and Apollo 17 landing sites.
2. The bulk compositions of the glass beads indicate that they originated from primary magma derived from the lunar mantle. The source region of the glass beads is estimated to have temperatures ranging from 1398 to 1436°C and pressures ranging from 8.3 to 11.9 kbar, corresponding to a depth range of 166–238 km within the lunar mantle. The source region is consistent with a depleted source characterized by dominant phases of olivine and orthopyroxene. Notably, the source region of the glass beads in NWA 11801 differs significantly from that of the Apollo glass beads, providing new insights into the heterogeneity of the lunar mantle.
3. The parental magma of glass beads ascended along a non-adiabatic path with an ascent rate of ~ 40 m s^{-1} or 0.2 MPa s^{-1}. During the ascent, olivine began to crystallize at ~ 1400°C and ~ 11 kbar (~ 220 km), and is the sole crystalline phase in the magma.
4. The glass beads experienced rapid cooling upon reaching the lunar surface, with estimated cooling rates ranging from 20 to 200 K min^{-1}. The cooling rate range is consistent with the typical cooling rates during flight along the ballistic trajectories of explosive volcanism.

Acknowledgments—The authors would like to express their gratitude to Bradley L. Jolliff and Anthony Gargano for their thorough, valuable, and constructive suggestions. The authors also acknowledge the contributions of Timothy Jull and Jeff Plescia for their meticulous editorial work. The authors thank Editsprings (https://www.editsprings.cn) for their professional English language editing. This research was financially supported by the National Natural Science Foundation of China (Grant Nos. 42203048, 41866008, 41776196, 42272348), Guangxi Scientific Base and Talent Special Projects (Grant Nos. AD23026084, AD1850007, AD23026339), Natural Science Foundation of Guangxi (Grant Nos. 2022GXNSFAA035567, 2021GXNSFBA075061), Innovation Project of Guangxi Graduate Education (YCBZ 2023144). [Correction added on 07 Sep 2023, after first online publication: Funding number '2203048' was changed to '42203048,'.]

Conflict of Interest Statement—The authors declare that they have no conflict of interest.

Data Availability Statement—The data that support the findings of this study are available in the supplementary material of this article.

Editorial Handling—Dr. Jeffrey Plescia

REFERENCES

Arndt, J., Engelhardt, W., Gonzalez-Cabeza, I., and Meier, B. 1984. Formation of Apollo 15 Green Glass Beads. *Journal of Geophysical Research: Solid Earth* 89: C225–C232. https://doi.org/10.1029/JB089iS01p0C225.

Arndt, J., and von Engelhardt, W. 1987. Formation of Apollo 17 Orange and Black Glass Beads. *Journal of Geophysical Research* 92: E372–E376. https://doi.org/10.1029/JB092iB04p0E372.

Basaltic Volcanism Study Project. 1981. *Basaltic Volcanism on the Terrestrial Planets*. New York: Pergamon Press, Inc.

Bechtold, A., Schulz, T., Wegner, W., Mader, D., Patterer, C., and Koeberl, C. 2022. Geochemistry of Lunar Meteorite Northwest Africa 11962 and its Potential Source Region/Crater in the Procellarum KREEP Terrane. *Meteoritics & Planetary Science* 57: 1688–1705. https://doi.org/10.1111/maps.13894.

Bennett, K., and Bell, J. F. 2023. Pyroclastic Deposits. In *Encyclopedia of Lunar Science*, edited by B. Cudnik. Cham: Springer. https://doi.org/10.1007/978-3-319-14541-9_117.

Brown, S. M., and Grove, T. L. 2015. Origin of the Apollo 14, 15, and 17 Yellow Ultramafic Glasses by Mixing of Deep Cumulate Remelts. *Geochimica et Cosmochimica Acta* 171: 201–215. https://doi.org/10.1016/j.gca.2015.09.001.

Chang, J., and Audétat, A. 2021. LA-ICP-MS Analysis of Crystallized Melt Inclusions in Olivine, Plagioclase, Apatite and Pyroxene: Quantification Strategies and Effects of Post-Entrapment Modifications. *Journal of Petrology* 62: egaa085. https://doi.org/10.1093/petrology/egaa085.

Chen, H.-K., Delano, J. W., and Lindsley, D. H. 1982a. Chemistry and Phase Relations of VLT Volcanic Glasses from Apollo 14 and Apollo 17. *Journal of Geophysical Research: Solid Earth* 87: A171–A181. https://doi.org/10.1029/JB087iS01p0A171.

Chen, H.-K., Delano, J. W., and Lindsley, D. H. 1982b. Liquidus-Phase Relations of the Apollo 14 and Apollo 17 VLT Volcanic Glasses (Abstract). *Lunar and Planetary Science XIII*: 84–85.

Chou, I. M., and Wang, A. 2017. Application of Laser Raman Micro-Analyses to Earth and Planetary Materials. *Journal of Asian Earth Sciences* 145: 309–333. https://doi.org/10.1016/j.jseaes.2017.06.032.

Costa, F., Dohmen, R., and Chakraborty, S. 2008. Time Scales of Magmatic Processes from Modeling the Zoning Patterns of Crystals. *Reviews in Mineralogy and Geochemistry* 69: 545–594. https://doi.org/10.2138/rmg.2008.69.14.

Day, J. M. D., Tait, K. T., Udry, A., Moynier, F., Liu, Y., and Neal, C. R. 2018. Martian Magmatism from Plume Metasomatized Mantle. *Nature Communications* 9: 4799. https://doi.org/10.1038/s41467-018-0719.

Delano, J. W. 1979. Apollo 15 Green Glass: Chemistry and Possible Origin. *10th Lunar and Planetary Science Conference* 1: 275–300.

Delano, J. W. 1986. Pristine Lunar Glasses: Criteria, Data, and Implications. *Journal of Geophysical Research* 91: D201–D213. https://doi.org/10.1029/JB091iB04p0D201.

Delano, J. W., and Livi, K. 1981. Lunar Volcanic Glasses and their Constraints on Mare Petrogenesis. *Geochimica et Cosmochimica Acta* 45: 2137–49. https://doi.org/10.1016/0016-7037(81)90066-1.

Demidova, S. I., Nazarov, M. A., Anand, M., and Taylor, L. A. 2003. Lunar Regolith Breccia Dhofar 287B: A Record of Lunar Volcanism. *Meteoritics & Planetary Science* 38: 501–514. https://doi.org/10.1111/j.1945-5100.2003.tb00023.x.

Donaldson, C. H. 1976. An Experimental Investigation of Olivine Morphology. *Contributions to Mineralogy and Petrology* 57: 187–213. https://doi.org/10.1007/BF00405225.

Elardo, S. M., Draper, D. S., and Shearer, C. K. 2011. Lunar Magma Ocean Crystallization Revisited: Bulk Composition, Early Cumulate Mineralogy, and the Source Regions of the Highlands Mg-Suite. *Geochimica et Cosmochimica Acta* 75: 3024–45. https://doi.org/10.1016/j.gca.2011.02.033.

Elkins-Tanton, L. T., Chatterjee, N., and Grove, T. L. 2003. Experimental and Petrological Constraints on Lunar Differentiation from the Apollo 15 Green Picritic Glasses. *Meteoritics & Planetary Science* 38: 515–527. https://doi.org/10.1111/j.1945-5100.2003.tb00024.x.

Elkins-Tanton, L. T., Fernandes, V. A., Delano, J. W., and Grove, T. L. 2000. Origin of Lunar Ultramafic Green Glasses: Constraints from Phase Equilibrium Studies. *Geochimica et Cosmochimica Acta* 64: 2339–50. https://doi.org/10.1016/S0016-7037(00)00365-3.

Fagan, T. J., Taylor, G. J., Keil, K., Bunch, T. E., Wittke, J. H., Korotev, R. L., Jolliff, B. L., et al. 2002. Northwest Africa 032: Product of Lunar Volcanism. *Meteoritics & Planetary Science* 37: 371–394. https://doi.org/10.1111/j.1945-5100.2002.tb00822.x.

Faure, F., Trolliard, G., Nicollet, C., and Montel, J. M. 2003. A Developmental Model of Olivine Morphology as a Function of Thecooling Rate and the Degree of Undercooling. *Contributions to Mineralogy and Petrology* 145: 251–263. https://doi.org/10.1007/s00410-003-0449-y.

Fink, J. H., and Griffiths, R. W. 1998. Morphology, Eruption Rates, and Rheology of Lava Domes: Insights from Laboratory Models. *Journal of Geophysical Research: Solid Earth* 103: 527–545. https://doi.org/10.1029/97JB02838.

Ghiorso, M. S., and Gualda, G. A. 2015. An H_2O–CO_2 Mixed Fluid Saturation Model Compatible with Rhyolite-MELTS. *Contributions to Mineralogy and Petrology* 169: 1–30. https://doi.org/10.1007/s00410-015-1141-8.

Goodrich, C. A., Treiman, A. H., Filiberto, J., Gross, J., and Jercinovic, M. 2013. K_2O-Rich Trapped Melt in Olivine in the Nakhla Meteorite: Implications for Petrogenesis of Nakhlites and Evolution of the Martian Mantle. *Meteoritics & Planetary Science* 48: 2371–2405. https://doi.org/10.1111/maps.12226.

Green, D. H., Ringwood, A. E., Ware, N. G., and Hibberson, W. O. 1974. Petrology and Petrogenesis of Apollo 17 Basalts and Apollo 17 Orange Glass (Abstract). In *Lunar Science V*, 287–89. Houston, TX: The Lunar Science Institute.

Grove, T. L., and Krawczynski, M. J. 2009. Lunar Mare Volcanism: Where Did the Magmas Come From? *Elements* 5: 29–34. https://doi.org/10.2113/gselements.5.1.29.

Gualda, G. A., Ghiorso, M. S., Lemons, R. V., and Carley, T. L. 2012. Rhyolite-MELTS: A Modified Calibration of MELTS Optimized for Silica-Rich, Fluid-Bearing Magmatic Systems. *Journal of Petrology* 53: 875–890. https://doi.org/10.1093/petrology/egr080.

Gudmundsson, A. 2012. Magma Chambers: Formation, Local Stresses, Excess Pressures, and Compartments. *Journal of Volcanology and Geothermal Research* 237: 19–41. https://doi.org/10.1016/j.jvolgeores.2012.05.015.

Haggerty, S. E. 1974. Apollo 17 Orange Glass: Textural and Morphological Characteristics of Devitrification. *5th Lunar and Planetary Science Conference* 1: 193–205.

Haupt, C. P., Renggli, C. J., Klaver, M., Steenstra, E. S., Berndt, J., Rohrbach, A., and Klemme, S. 2023. Experimental and Petrological Investigations into the Origin of the Lunar Chang'e 5 Basalts. *Icarus* 402: 115625. https://doi.org/10.1016/j.icarus.2023.115625.

Head, J. W., and Wilson, L. 2017. Generation, Ascent and Eruption of Magma on the Moon: New Insights into Source Depths, Magma Supply, Intrusions and Effusive/Explosive Eruptions (Part 2: Predicted Emplacement Processes and Observations). *Icarus* 283: 176–223. https://doi.org/10.1016/j.icarus.2016.05.031.

Heiken, G. H., McKay, D. S., and Brown, R. 1974. Lunar Deposits of Possible Pyroclastic Origin. *Geochimica et Cosmochimica Acta* 38: 1703–18. https://doi.org/10.1016/0016-7037(74)90187-2.

Herzberg, C., and Asimow, P. 2015. PRIMELT 3 MEGA. XLSM Software for Primary Magma Calculation: Peridotite Primary Magma MgO Contents from the Liquidus to the Solidus. *Geochemistry, Geophysics, Geosystems* 16: 563–578. https://doi.org/10.1002/2014GC005631.

Hess, P. C., and Parmentier, E. M. 1995. A Model for the Thermal and Chemical Evolution of the Moon's Interior: Implications for the Onset of Mare Volcanism. *Earth and Planetary Science Letters* 134: 501–514. https://doi.org/10.1016/0012-821X(95)00138-3.

Hiesinger, H., Head, J., Wolf, U., Jaumann, R., and Neukum, G. 2011. Ages and Stratigraphy of Lunar Mare Basalts: A Synthesis. *Recent Advances and Current Research Issues in Lunar Stratigraphy* 477: 1–51. https://doi.org/10.1130/2011.2477(01).

Holland, T. J., Green, E. C., and Powell, R. 2018. Melting of Peridotites through to Granites: A Simple Thermodynamic Model in the System KNCFMASHTOCr. *Journal of Petrology* 59: 881–900. https://doi.org/10.1093/petrology/egy048.

Howarth, G. H., and Gross, J. 2019. Diffusion-Controlled and Concentric Growth Zoning Revealed by Phosphorous in

Olivine from Rapidly Ascending Kimberlite Magma, Benfontein, South Africa. *Geochimica et Cosmochimica Acta* 266: 292–306. https://doi.org/10.1016/j.gca.2019.08.006.

Hui, H., Hess, K. U., Zhang, Y., Nichols, A. R., Peslier, A. H., Lange, R. A., Dingwell, D. B., and Neal, C. R. 2018. Cooling Rates of Lunar Orange Glass Beads. *Earth and Planetary Science Letters* 503: 88–94. https://doi.org/10.1016/j.epsl.2018.09.019.

Johnson, B. C., Andrews-Hanna, J. C., Collins, G. S., Freed, A. M., Melosh, H. J., and Zuber, M. T. 2018. Controls on the Formation of Lunar Multiring Basins. *Journal of Geophysical Research: Planets* 123: 3035–50. https://doi.org/10.1029/2018JE005765.

Jolliff, B. L., Wieczorek, M. A., Shearer, C. K., and Neal, C. R. 2006. *In New Views of the Moon*, Vol. 60. http://www.minsocam.org/msa/rim/rim60.html.

Jurewicz, A. J., and Watson, E. B. 1988. Cations in Olivine, Part 2 Diffusion in Olivine Xenocrysts, with Applications to Petrology and Mineral Physics. *Contributions to Mineralogy and Petrology* 99: 186–201. https://doi.org/10.1007/BF00371460.

Keske, A. L., Clarke, A. B., and Robinson, M. S. 2020. On the Eruptive Origins of Lunar Localized Pyroclastic Deposits. *Earth and Planetary Science Letters* 547: 116426. https://doi.org/10.1016/j.epsl.2020.116426.

Klaver, M., Luu, T. H., Lewis, J., Jansen, M. N., Anand, M., Schwieters, J., and Elliott, T. 2021. The Ca Isotope Composition of Mare Basalts as a Probe into the Heterogeneous Lunar Mantle. *Earth and Planetary Science Letters* 570: 117079. https://doi.org/10.1016/j.epsl.2021.117079.

Kuskov, O. L., Kronrod, E. V., and Kronrod, V. A. 2019. Thermo-Chemical Constraints on the Lunar Bulk Composition and the Structure of a Three-Layer Mantle. *Physics of the Earth and Planetary Interiors* 286: 1–12. https://doi.org/10.1016/j.pepi.2018.10.011.

Kuzmin, D. V., and Sobolev, A. V. 2003. Boundary Layer Effect on the Composition of Melt Inclusions in Olivine. *EGS-AGU-EUG Joint Assembly*, p. 5665.

Lasaga, A. C. 1981. Implications of a Concentration-Dependent Growth Rate on the Boundary Layer Crystal-Melt Model. *Earth and Planetary Science Letters* 56: 429–434. https://doi.org/10.1016/0012-821X(81)90146-1.

Lee, C. T. A., Luffi, P., Plank, T., Dalton, H., and Leeman, W. P. 2009. Constraints on the Depths and Temperatures of Basaltic Magma Generation on Earth and Other Terrestrial Planets Using New Thermobarometers for Mafic Magmas. *Earth and Planetary Science Letters* 279: 20–33. https://doi.org/10.1016/j.epsl.2008.12.020.

Li, Q. L., Zhou, Q., Liu, Y., Xiao, Z. Y., Lin, Y. T., Li, J. H., Ma, H. X., et al. 2021. Two-Billion-Year-Old Volcanism on the Moon from Chang'e-5 Basalts. *Nature* 600: 54–58. https://doi.org/10.1038/s41586-021-04100-2.

Longhi, J., Walker, D., and Hays, J. F. 1978. The Distribution of Fe and Mg between Olivine and Lunar Basaltic Liquids. *Geochimica et Cosmochimica Acta* 42: 1545–58. https://doi.org/10.1016/0016-7037(78)90025-X.

Lucey, P., Korotev, R. L., Gillis, J. J., Taylor, L. A., Lawrence, D., Campbell, B. A., Elphic, R., et al. 2006. Understanding the Lunar Surface and Space-Moon Interactions. *Reviews in Mineralogy and Geochemistry* 60: 83–219. https://doi.org/10.2138/rmg.2006.60.2.

McCallum, I. S., and O'Brien, H. E. 1996. Stratigraphy of the Lunar Highland Crust; Depths of Burial of Lunar Samples from Cooling-Rate Studies. *American Mineralogist* 81: 1166–75. https://doi.org/10.2138/am-1996-9-1015.

McCubbin, F. M., Vander Kaaden, K. E., Tartèse, R., Klima, R. L., Liu, Y., Mortimer, J., Barnes, J. J., et al. 2015. Magmatic Volatiles (H, C, N, F, S, Cl) in the Lunar Mantle, Crust, and Regolith: Abundances, Distributions, Processes, and Reservoirs. *American Mineralogist* 100: 1668–1707. https://doi.org/10.2138/am-2015-4934CCBYNCND.

Misener, D. J. 1974. Cationic Diffusion in Olivine to 1400°C and 35 kbar. In *Geochemical Transport and Kinetic*, edited by A. W. Hofmann, B. J. Giletti, Y. H. S. Jr., and R. A. Yund, 117–129. Washington, DC: Carnegie Institute Press. https://doi.org/10.14288/1.0302660.

Mollo, S., and Hammer, J. E. 2017. Dynamic Crystallization in Magmas. *EMU Notes Mineral* 16: 373–418. https://doi.org/10.1180/EMU-notes.16.12.

Montazerian, M., and Zanotto, E. D. 2022. Nucleation, Growth, and Crystallization in Oxide Glass-Formers. A Current Perspective. *Reviews in Mineralogy and Geochemistry* 87: 405–429. https://doi.org/10.2138/rmg.2022.87.09.

Morgan, C., Wilson, L., and Head, J. W. 2021. Formation and Dispersal of Pyroclasts on the Moon: Indicators of Lunar Magma Volatile Contents. *Journal of Volcanology and Geothermal Research* 413: 107217. https://doi.org/10.1016/j.jvolgeores.2021.107217.

Mouri, T., and Enami, M. 2008. Raman Spectroscopic Study of Olivine-Group Minerals. *Journal of Mineralogical and Petrological Sciences* 103: 100–104. https://doi.org/10.2465/jmps.071015.

Naney, M. T., Crowl, D. M., and Papike, J. J. 1976. The Apollo 16 Drill Core: Statistical Analysis of Glass Chemistry and the Characterization of a High Alumina-Silica Poor (HASP) Glass. *7th Lunar and Planetary Science Conference*, pp. 155–184.

Nicholis, M. G., and Rutherford, M. J. 2009. Graphite Oxidation in the Apollo 17 Orange Glass Magma: Implications for the Generation of a Lunar Volcanic Gas Phase. *Geochimica et Cosmochimica Acta* 73: 5905–17. https://doi.org/10.1016/j.gca.2009.06.022.

Papike, J. J., Shearer, C. K., and Galbreath, K. C. 1990. Reading the Moon's Volcanic Record by Ion Microprobe Analysis of Apollo 14 Glass Beads. *Geology* 18: 295–98. https://doi.org/10.1130/0091-7613(1990)018<0295:RTMSVR>2.3.CO;2.

Putirka, K. D. 2008. Thermometers and Barometers for Volcanic Systems. *Reviews in Mineralogy and Geochemistry* 69: 61–120. https://doi.org/10.2138/rmg.2008.69.3.

Renggli, C. J., King, P. L., Henley, R. W., and Norman, M. D. 2017. Volcanic Gas Composition, Metal Dispersion and Deposition during Explosive Volcanic Eruptions on the Moon. *Geochimica et Cosmochimica Acta* 206: 296–311. https://doi.org/10.1016/j.gca.2017.03.012.

Richter, F., Saper, L. M., Villeneuve, J., Chaussidon, M., Watson, E. B., Davis, A. M., Mendybaev, R. A., and Simon, S. B. 2021. Reassessing the Thermal History of Martian Meteorite Shergotty and Apollo Mare Basalt 15555 Using Kinetic Isotope Fractionation of Zoned Minerals. *Geochimica et Cosmochimica Acta* 295: 265–285. https://doi.org/10.1016/j.gca.2020.11.002.

Rothery, D. A., Glaze, L. S., and Wilson, L. 2022. Explosive Volcanism: Observations and Processes. *Planetary*

Volcanism Across the Solar System 1: 115–160. https://doi.org/10.1016/B978-0-12-813987-5.00004-3.

Rutherford, M. J., Head, J. W., Saal, A. E., Hauri, E., and Wilson, L. 2017. Model for the Origin, Ascent, and Eruption of Lunar Picritic Magmas. *American Mineralogist: Journal of Earth and Planetary Materials* 102: 2045–53. https://doi.org/10.2138/am-2017-5994ccbyncnd.

Saal, A. E., and Hauri, E. H. 2021. Large Sulfur Isotope Fractionation in Lunar Volcanic Glasses Reveals the Magmatic Differentiation and Degassing of the Moon. *Science Advances* 7: eabe4641. https://doi.org/10.1126/sciadv.abe4641.

Shearer, C. K., Hess, P. C., Wieczorek, M. A., Pritchard, M. E., Parmentier, E. M., Borg, L. E., Longhi, J., et al. 2006. Thermal and Magmatic Evolution of the Moon. *Reviews in Mineralogy and Geochemistry* 60: 365–518. https://doi.org/10.2138/rmg.2006.60.4.

Shearer, C. K., and Papike, J. J. 1993. Basaltic Magmatism on the Moon: A Perspective from Volcanic Picritic Glass Beads. *Geochimica et Cosmochimica Acta* 57: 4785–4812. https://doi.org/10.1016/0016-7037(93)90200-G.

Su, B., Yuan, J. Y., Chen, Y., Yang, W., Mitchell, R. N., Hui, H. J., Wang, H., Tian, H. C., Li, X. H., and Wu, F. Y. 2022. Fusible Mantle Cumulates Trigger Young Mare Volcanism on the Cooling Moon. *Science Advances* 8: eabn2103. https://doi.org/10.1126/sciadv.abn2103.

Walker, D., Hager, B., and Hayes, J. 1980. Mass and Heat Transport in a Lunar Magma Ocean by Sinking Blobs. *Lunar and Planetary Science Conference XI*, pp. 1196–98. https://ui.adsabs.harvard.edu/abs/1980LPI....11.1196W/abstract

Walker, D., Longhi, J., Stolper, E. M., Grove, T. L., and Hays, J. F. 1975. Origin of Titaniferous Lunar Basalts. *Geochimica et Cosmochimica Acta* 39: 1219–35. https://doi.org/10.1016/0016-7037(75)90129-5.

Weitz, C. M., Rutherford, M. J., Head, J. W., III, and McKay, D. S. 1999. Ascent and Eruption of a Lunar High-Titanium Magma as Inferred from the Petrology of the 74001/2 Drill Core. *Meteoritics & Planetary Science* 34: 527–540. https://doi.org/10.1111/j.1945-5100.1999.tb01361.x.

Whitney, D. L., and Evans, B. W. 2010. Abbreviations for Names of Rock-Forming Minerals. *American Mineralogist* 95: 185–87. https://doi.org/10.2138/am.2010.3371.

Wieczorek, M. A., Jolliff, B. L., Khan, A., Pritchard, M. E., Weiss, B. P., Williams, J. G., Hood, L. L., et al. 2006. The Constitution and Structure of the Lunar Interior. *Reviews in Mineralogy and Geochemistry* 60: 221–364. https://doi.org/10.2138/rmg.2006.60.3.

Wilson, L., and Head, J. W. 1981. Ascent and Eruption of Basaltic Magma on the Earth and Moon. *Journal of Geophysical Research* 86: 2971–3001. https://doi.org/10.1029/JB086iB04p02971.

Wilson, L., and Head, J. W. 1983. A Comparison of Volcanic Eruption Processes on Earth, Moon, Mars, Io, and Venus. *Nature* 302: 663–69. https://doi.org/10.1038/302663a0.

Wilson, L., and Head, J. W. 2003. Deep Generation of Magmatic Gas on the Moon and Implications for Pyroclastic Eruptions. *Geophysical Research Letters* 30: 1605. https://doi.org/10.1029/2002GL016082.

Wilson, L., and Head, J. W. 2017. Generation, Ascent and Eruption of Magma on the Moon: New Insights into Source Depths, Magma Supply, Intrusions and Effusive/Explosive Eruptions (Part 1: Theory). *Icarus* 283: 146–175. https://doi.org/10.1016/j.icarus.2015.12.039.

Wilson, L., and Head, J. W. 2018. Controls on Lunar Basaltic Volcanic Eruption Structure and Morphology: Gas Release Patterns in Sequential Eruption Phases. *Geophysical Research Letters* 45: 5852–59. https://doi.org/10.1029/2018GL078327.

Xiang, H., and Connolly, J. A. 2021. GeoPS: An Interactive Visual Computing Tool for Thermodynamic Modelling of Phase Equilibria. *Journal of Metamorphic Geology* 40: 243–255. https://doi.org/10.1111/jmg.12626.

Zellner, N. E. B., Delano, J. W., Swindle, T. D., Barra, F., Olsen, E., and Whittet, D. C. B. 2009. Apollo 17 Regolith, 71501,262: A Record of Impact Events and Mare Volcanism in Lunar Glasses. *Meteoritics & Planetary Science* 44: 839–851. https://doi.org/10.1111/j.1945-5100.2009.tb00772.x.

Zeng, X., Li, X., Liu, J., Mo, B., Yu, W., and Tang, H. 2020. Discerning Lunar Pyroclastic and Impact Glasses Via Raman Spectroscopy. *Journal of Geophysical Research (Planets)* 125: e06674. https://doi.org/10.1029/2020JE006674.

Zeng, X., Li, X., Martin, D., Tang, H., Yu, W., Liu, J., and Wang, S. 2019. Micro-FTIR Spectroscopy of Lunar Pyroclastic and Impact Glasses as a New Diagnostic Tool to Discern Them. *Journal of Geophysical Research (Planets)* 124: 3267–82. https://doi.org/10.1029/2019JE006237.

Zeng, X., Li, X., Xia, X. P., Liu, J., Cui, Z., Yu, W., and Ouyang, Z. 2021. New Evidence for 4.32 Ga Ancient Silicic Volcanism on the Moon. *Geophysical Research Letters* 48: e92639. https://doi.org/10.1029/2021GL092639.

SUPPORTING INFORMATION

Additional supporting information may be found in the online version of this article.

TABLE S1. The chemical composition of studied volcanic glass beads in NWA 11801 (wt%).

TABLE S2. The chemical composition of olivines in volcanic glass (VG-2) (wt%).

TABLE S3. The chemical composition of melt inclusions in olivines (wt%).